Princeton Plasma Physics Laboratory

PPPL- 4314

PPPL- 4314

Electron Bernstein Wave Emission and Mode Conversion Physics on NSTX

S.J. Diem, G. Taylor, J.B. Caughman, P. Efthimion, H. Kugel, B.P. LeBlanc, J. Preinhaelter, S.A. Sabbagh, J. Urban, and J. Wilgen

May 2008

Prepared for the U.S. Department of Energy under Contract DE-AC02-76CH03073.

Princeton Plasma Physics Laboratory
Report Disclaimers

Full Legal Disclaimer

Trademark Disclaimer

PPPL Report Availability

Princeton Plasma Physics Laboratory:

http://www.pppl.gov/techreports.cfm

Office of Scientific and Technical Information (OSTI):

http://www.osti.gov/bridge

Related Links:

U.S. Department of Energy

Office of Scientific and Technical Information

Fusion Links

Electron Bernstein Wave Emission and Mode Conversion Physics on NSTX

S.J. Diem[1], G. Taylor[1], J.B. Caughman[2], P. Efthimion[1], H. Kugel[1], B.P. LeBlanc[1], J. Preinhaelter[3], S.A. Sabbagh[4], J. Urban[3], J. Wilgen[2]

1) Princeton Plasma Physics Laboratory, P.O. Box 451, Princeton, NJ 08543, USA

2) Oak Ridge National Laboratory, Fusion Energy Division, P.O. Box 2008, Oak Ridge, TN 37831-6169, USA

3) EURATOM/IPP.CR Association, Institute of Plasma Physics, 18200 Prague 8, Czech Republic

4) Columbia University, Department of Applied Physics and Applied Mathematics, New York, NY 10027, USA

Abstract: NSTX is a spherical tokamak (ST) that operates with n_e up to 10^{20} m^{-3} and B_T less than 0.6 T, cutting off low harmonic electron cyclotron (EC) emission widely used for T_e measurements on conventional aspect ratio tokamaks. The electron Bernstein wave (EBW) can propagate in ST plasmas and is emitted at EC harmonics. These properties suggest thermal EBW emission (EBE) may be used for local T_e measurements in the ST. Practically, a robust $T_e(R,t)$ EBE diagnostic requires EBW transmission efficiencies of > 90% for a wide range of plasma conditions. EBW emission and coupling physics were studied on NSTX with an obliquely viewing EBW to O-mode (B-X-O) diagnostic with two remotely steered antennas, coupled to absolutely calibrated radiometers. While $T_e(R,t)$ measurements with EBW emission on NSTX were possible, they were challenged by several issues. Rapid fluctuations in edge n_e scale length resulted in > 20% changes in the low harmonic B-X-O transmission efficiency. Also, B-X-O transmission efficiency

during H-modes was observed to decay by a factor of 5-10 to less than a few percent. The B-X-O transmission behavior during H-modes was reproduced by EBE simulations that predict that EBW collisional damping can significantly reduce emission when $T_e < 30$ eV inside the B-X-O mode conversion (MC) layer. Initial edge lithium conditioning experiments during H-modes have shown that evaporated lithium can increase T_e inside the B-X-O MC layer, significantly increasing B-X-O transmission.

I. INTRODUCTION

Spherical tokamaks (STs) routinely operate with plasmas that have high electron densities, n_e, and low toroidal magnetic fields, B_T, such that the plasmas are overdense, $\omega_{pe} >> \Omega_{ce}$, where ω_{pe} is the electron plasma frequency and Ω_{ce} is the electron cyclotron frequency. Traditionally, tokamaks and many other magnetically confined plasmas devices have utilized electron cyclotron (EC) waves to provide local electron temperature, T_e, measurements via electron cyclotron emission (ECE) [1]. In these overdense devices, the propagation of low harmonic EC waves beyond the plasma edge is cutoff, prohibiting the use of ECE for T_e measurements. The National Spherical Torus Experiment (NSTX) [2] routinely studies plasma in the overdense regime, with n_e up to 10^{20} m^{-3} and $B_t < 0.6$ T, so that ECE at the first five EC harmonics is cutoff. An alternative to EC waves in this overdense regime is the electrostatic electron Bernstein wave (EBW) [3], which propagates mainly perpendicular to the external magnetic field and is strongly emitted near EC harmonics. Unlike electromagnetic EC waves, EBWs do not experience a density cutoff in the plasma. The EBW cannot propagate in vacuum, but must couple to an ordinary (O) or extraordinary (X) electromagnetic wave in order to be

detected by a receiving antenna located outside of the vacuum vessel. Coupling to the EBW can be achieved through two mode conversion schemes: B-X (EBW to X-mode coupling) [4] and the double mode conversion process of B-X-O (EBW to X-mode to O-mode coupling) mode conversion [5]. Currently, NSTX is studying thermal emission via B-X-O mode conversion. In this conversion process thermal EBW emission (EBE), generated near an EC harmonic resonance, travels towards the plasma edge until it mode converts to the slow X-mode at the upper hybrid resonance (UHR) layer where $\omega = ((\omega_{pe})^2+(\Omega_{ce})^2)^{1/2}$. At the UHR layer, the perpendicular wave vector, $k_\perp$, of the EBW and the slow X-mode branch are equal and full conversion between the two branches occurs. The slow X-mode propagates back into the plasma until it encounters the left-hand cutoff of the X-mode (where $\omega = (1/2)[-\Omega_{ce}+(\Omega_{ce}^2+4\omega_{pe}^2)^{1/2}]$). For particular oblique viewing angles, the left-hand cutoff of the slow X-mode branch is coincident with the O-mode cutoff (where $\omega = \omega_{pe}$) and the power in the slow X-mode is transferred to the O-mode branch. The B-X-O mode conversion efficiency is given by [6,7]:

$$T\left(n_\perp, n_\parallel\right) = \exp\left(-\pi k_o L_n \sqrt{(Y/2)}\left[2(1+Y)\left(n_{\parallel,opt} - n_\parallel\right)^2 + n_\perp^2\right]\right) \quad (1a)$$

$$n_{\parallel,opt}^2 = \left(\frac{Y}{Y+1}\right) = \cos^2\left(\phi_{opt}\right) \quad (1b)$$

$$Y = \left(\frac{\Omega_{ce}}{\omega}\right) \quad (1c)$$

In the equations above, $n_\parallel$ and $n_\perp$ are the parallel and perpendicular indices of refraction, respectively, and L_n is the density scale length evaluated at the UHR. An example of the calculated B-X-O mode conversion efficiency window for an NSTX plasma is shown in figure 1. Two angular emission windows are available for a given frequency: one along

the magnetic field (positive angles) and the other against the magnetic field (negative angles). The center of the B-X-O transmission window in poloidal and toroidal angle depends on the magnetic field and the magnetic field pitch at the mode conversion (MC) layer. L_n at the MC layer determines the angular width of the window. By decreasing L_n, the angular width of the window is increased. The B-X-O mode conversion efficiency in equation (1a) only calculates the mode conversion at the O-mode cutoff layer and does not account for re-absorption and re-emission prior to B-X-O conversion. An EBE simulation code was used to calculate these losses.

This paper presents details of EBE measurements made via B-X-O mode conversion on NSTX and discusses the challenges for reconstructing $T_e(R)$ from these measurements. Section II describes the B-X-O emission diagnostic used on NSTX and the EBE simulation code used to interpret the emission measurements. Section III.A presents results that show the effect of density fluctuations on the B-X-O transmission, section III.B presents results that show the effect of EBW collisional damping and in section III.C a $T_e(R)$ profile is reconstructed from the emission. The implications of the results are discussed in section IV.

II. EBE DIAGNOSTIC AND SIMULATION CODE

EBE measurements on NSTX are acquired with two remotely steered, quad-ridged microwave antennas measuring fundamental, second and third harmonic emission in the frequency range 8-36 GHz [8]. The antennas are mounted outside of the vacuum vessel, 50 cm from the plasma edge. The antenna ridges are oriented to measure emission polarization components perpendicular and parallel to the magnetic field at the MC layer.

The total radiation temperature, T_{rad}, is determined by adding the two polarization components together. Each antenna mount has two linear actuators to control movement in the poloidal and toroidal directions, allowing a scan of the B-X-O transmission window. The antennas are each coupled to a dual-channel heterodyne radiometer, one measuring 8-18 GHz and the other 18-36 GHz emission. This paper will only present emission results from the 18-36 GHz radiometer range. A quad-ridged microwave horn antenna (Q-par Angus Ltd., model number WBH18-40DPK) with a broadband frequency coverage of 18-40 GHz was coupled to the 18-36 GHz radiometer utilizing a Miteq SBE0440LW1 second harmonic mixer (figure 2). The frequency coverage is achieved via two separate voltage-controlled oscillators (VCOs): one with a range of 8 to 12 GHz and the second with a range of 12-18 GHz. The two VCOs are alternately activated via a TTL logic controlled switch (American Microwave Corp. SPDT 8-18 GHz switch, shown in figure 3). The VCOs are frequency scanned at 10 kHz, via an Agilent 33120A Waveform Generator, to measure the evolution of the emission spectrum. The radiometers are absolutely calibrated using the Dicke switching method [9].

The optical depth for EBWs at low harmonic EC resonances is ~ 3000 in NSTX, well satisfying the blackbody condition, so the measured T_{rad} can be assumed to be equal to the local T_e, provided the B-X-O mode conversion efficiency is ~100%. For cases where the B-X-O mode conversion efficiency is not equal to 100%, EBE simulations were used to deduce T_e.

The emission measurements were simulated with an EBE numerical code developed by Preinhaelter and Urban [10]. The code simulates the process of O-X-B injection; however, due to the reciprocity of the injection and emission processes [11],

the absorption and emission location are the same. A bundle of 41 rays are launched in the code to simulate the antenna pattern of the EBE diagnostic. A full-wave code [12] calculates the mode conversion efficiency of the O-X-B mode conversion assuming a 1-D plasma slab model. A 3-D ray-tracing code calculates the propagation and absorption of the EBW after mode conversion. The EBE code uses the T_e and n_e profiles measured by laser Thomson scattering [13] and the magnetic equilibrium reconstructed by EFIT [14]. Collisions are incorporated into the EBE code with a BGK collision operator [15, 16].

III. EBE MEASUREMENTS AND SIMULATIONS

A viable EBE $T_e(R,t)$) diagnostic requires the EBW transmission in the plasma and mode conversion to electromagnetic radiation to be efficient, or at least well characterized. EBW research on NSTX has focused on investigating EBE via B-X-O coupling to evaluate its use for reconstructing a $T_e(R)$ profile, specifically the effect of density fluctuations (section III.A) and EBW collisional damping (section III.B) on B-X-O transmission efficiency. Being able to quantify these effects allows B-X-O coupled thermal EBE to be used for the reconstruction of the $T_e(R)$ profile (section III.C).

A. Effects of density fluctuations in T_{rad}

The EBE T_{rad} measurements on NSTX all exhibited a large, up to 90%, fluctuation during both L-mode and H-mode plasmas, as shown in figure 4 (a) for fundamental emission from an L-mode discharge. The thermal noise fluctuation level for the NSTX EBE diagnostic is calculated to only be ~14%, much lower than the measured fluctuation in T_{rad}. This suggests that the fluctuations in T_{rad} are either due to fluctuations

in T_e at the emission location or due to fluctuations in n_e at the MC layer that result in fluctuations in the B-X-O mode conversion efficiency. The MC layer for fundamental EBW conversion is typically located within several centimeters of the last closed flux surface (LCFS). Data from an edge density reflectometer [17] was used to compute L_n at the MC layer for the shot shown in figure 4. L_n ranged from 1 cm to 6 cm during the plasma current flattop (dashed line in figure 4 (b)). The measured L_n was inserted into equation (1a) to estimate the fluctuation in B-X-O mode conversion efficiency. The calculated B-X-O mode conversion efficiency for this case ranges from 70-90%, agreeing with the measured value of 90±15%. The measured L_n fluctuation level results in a ~25% fluctuation in the B-X-O mode conversion efficiency (solid line in figure 4 (b)). When reconstructing $T_e(R)$, the maximum value of the measured T_{rad} was used.

B. Effects of EBW collisional damping on EBE

Good B-X-O coupling in H-mode plasmas is especially important for ST devices that routinely operate in an overdense H-mode regime. However, while good fundamental B-X-O transmission was measured for L-mode plasmas [18], early EBE measurement in NSTX H-mode plasmas revealed very low B-X-O transmission efficiencies of only a few percent during the plasma current flattop phase of the discharge. The B-X-O transmission efficiency, $\eta_{B\text{-}X\text{-}O}$, accounts for all the EBW losses due to re-absorption, re-emission, and mode conversion the EBW experiences between the point where it is emitted and when it is detected. During initial B-X-O emission measurements in H-mode plasmas, B-X-O transmission efficiencies were 20-60% for f_{ce}, $2f_{ce}$ and $3f_{ce}$ (18-36 GHz) emission at the L-H transition, but decayed to a few percent

during the H-mode phase (figure 5 (b)). Preinhaelter et al. [10] first suggested EBW collisional damping [19] as the cause for the observed decay in EBE seen in NSTX H-mode plasmas. EBW collisional damping can become important if the local T_e between the emitting EC layer and the MC is less than 30 eV. For these temperatures, the local collision frequency can be high enough that the EBW experiences significant collisional damping, resulting in little or no EBW power being converted to the X- and O-mode. For times prior to t = 0.25 s (for the case shown in figure 5), the second harmonic B-X-O MC layer is located within 1 cm of the LCFS where $T_e > 20$ eV. For times greater than 0.25 s for this discharge, the MC layer is shifted 3 to 9 centimeters outside of the LCFS where T_e is lower than 10 eV. EBE simulations for 18 GHz fundamental emission of this plasma without incorporating EBW collisional damping prior to MC predict a relatively constant value of $T_{rad} \sim 0.8$ keV, significantly larger than the measured T_{rad} of less than 20 eV. When collisional damping of EBWs prior to MC is included, the simulations reproduce the measured T_{rad} decay during H-mode, shown in Fig. 5(b). The EBE simulations predict that the collision frequency near the MC layer increases over a factor of 3 for times greater than t = 0.25 s and as a result the emission power decreases over a factor of 3. The very low B-X-O transmission efficiencies observed during H-mode plasmas (figure 5 (b)) make EBE $T_e(R)$ measurement impossible. These results also suggest that if the edge collisionality can be reduced it may be possible to reconstruct a temperature profile from EBE measurements. One method of reducing the edge collisionality is through lithium edge conditioning.

On NSTX lithium evaporation [20] has been used to reduce the density in the plasma scrape off and in the vicinity of the LCFS. For H-mode discharges without

lithium conditioning, the MC layer for fundamental EBE was typically located > 5 cm outside of the LCFS, where $T_e < 10$ eV. A lithium evaporation rate of 19 mg/min was used to reduce n_e by a factor of 2 in the plasma scrape off so that the MC layer was moved to the LCFS where $T_e > 20$ eV. With edge conditioning the emission remained at a constant level throughout the H-mode phase of the discharge (solid line in figure 6). For 18 GHz fundamental EBE, the B-X-O transmission efficiency increased from a few percent with no lithium conditioning to 60% with lithium conditioning. Similarly, the B-X-O transmission efficiency for second harmonic emission increased from a few percent to 50% with the addition of lithium edge conditioning. The use of edge conditioning reduced the EBW power lost to collisional damping to only 20%, as compared to 90% without edge conditioning. Good agreement between the measured and simulated T_{rad} with collisions was observed (figure 6), allowing the B-X-O transmission efficiency to be calculated for use in reconstructing the $T_e(R)$ profile.

C. T_e reconstruction

To reconstruct the $T_e(R)$ profile using EBE data, the ray-tracing code contained in the EBE simulation code was used to map the emission frequency to an emission radius, $R_{emission}$. The time evolution of the plasma current, central electron temperature and density for this plasma are shown in figure 7. The time of t = 0.365 s was chosen to reconstruct the T_e profile because it was well into the plasma current flattop when all global parameters had become quasi-stationary. The emission frequency ranges measured were 18-22 GHz and 26-32 GHz. This frequency range provided T_{rad} measurements from major radius, R = 0.8-1.45 m; however, the $R_{emission}$ for these frequency ranges was

primarily from near the plasma magnetic axis (R_0 = 1.0 m) and the plasma edge (R > 1.4 m).

The reconstructed $T_e(R)$ from the EBE measurements is shown as a function of major radius in figure 8 and is compared to the $T_e(R)$ profile measured by laser Thomson scattering. T_e is reconstructed from the measured T_{rad} by dividing the measured T_{rad} by the simulated B-X-O transmission efficiency, $\eta_{B\text{-}X\text{-}O}$. The simulated B-X-O transmission efficiency accounts for all of the losses due to re-absorption and re-emission, as well as losses due to EBW collisional damping prior to mode conversion. The emission radius was taken to be a weighted average of the emission radius for the 41 rays used to simulate the antenna beam waist in the EBE simulation. The radial error bars in figure 8 represent one weighted standard deviation of the emission location for the 41 rays. The vertical error bars represent the uncertainty in the T_{rad} measurement. Highly localized emission is seen for emission locations in the region R > 1.41 m. The large radial spread for T_{rad} from R < 1.4 m can be attributed to emission simultaneously coming from the fundamental and second harmonic, so that the emission location varied between 0.8 m and 1.5 m for the 41 rays (figure 9). Good agreement is observed between T_{rad} and the Thomson scattering edge profile for R > 1.4 m. EBWs emitted from the plasma edge have much less plasma to propagate through; therefore, there is less power loss of the EBW due to re-absorption and re-emission. In addition, there is less harmonic overlap for edge emission (as seen in figure 10), so the emission is much more highly localized. All of the emission from the plasma edge comes from a region no more than 2 cm in radial width (figure 11). The radial extent of the core emission is anywhere from 2 cm to 15 cm,

as indicated by the radial bars in figure 8 and shown in detail for 28 GHz emission in figure 11.

IV. DISCUSSION

Measuring the $T_e(R)$ profile via B-X-O emission measurements in the ST is difficult. The B-X-O process is complicated, involving double mode conversion of the emission before it is detected, and an antenna view oblique to the magnetic field near the plasma edge, so that extensive numerical modeling is needed to determine the emission location and hence reconstruct the $T_e(R)$ profile. In contrast to stellallators or conventional aspect ratio tokamaks, reconstruction of the magnetic equilibrium in an ST is strongly affected by time varying internal currents that generate poloidal fields that can be comparable to the toroidal field. In addition, significant Doppler broadening can lead to re-absorption and re-emission of the radiation as it travels through the plasma. Although the EBE simulation code provides a method to calculate these losses and determine the emission location used for $T_e(R)$ reconstructions, the code results are very sensitive to the reconstructed magnetic equilibrium from EFIT and the T_e and n_e profiles from Thomson scattering. An accurate description of the antenna pattern of the EBE diagnostic and its orientation is also required for accurate EBE simulations. If any of these input data are inaccurate, the emission location of the EBWs will not be correctly calculated, and the $T_e(R)$ profile will be poorly reconstructed. In addition, density fluctuations at the B-X-O MC layer lead to large fluctuations in the B-X-O transmission efficiency and EBW collisional damping can significantly reduce the B-X-O transmission efficiency or sometimes entirely absorb the EBW before mode conversion occurs.

Lithium edge conditioning has been used successfully to mitigate the EBW collisional damping and as a result increase EBW coupling efficiency to 60%.

ACKNOWLEDGEMENTS

Research supported by USDOE DE-AC02-76CH03073, DE-FG02-91ER-54109, DE-FG03-02ER-54684, DE-FG02-99ER-54521 and a grant to encourage innovations in fusion diagnostic systems. The authors would like to thank L. Guttadora and P. Roney for their help in developing the NSTX EBW emission diagnostic and C.K. Phillips for useful discussions.

REFERENCES

1. M.R. Bornatici, R. Cano, O. De Barbiere, and F. Englemann, *Nucl. Fusion* **23**, 1153 (1983).

2. M. Ono, et al., *Nucl. Fusion*, **40** (2000).

3. I.B. Bernstein, *Phys. Rev. Lett.* **109**, 10 (1958).

4. A.K. Ram and S.D. Schultz, *Phys. of Plasmas* **7**, 4084 (2000).

5. J. Preinhaelter and V. Kopecky, *J. Plasma Phys*. **10**, 1 (1973).

6. E. Mjϕlhus, *J. Plasma Phys.* **31**, 7 (1984).

7. F.R. Hansen, J.P. Lynoc, C. Maroli, and V. Petrillo, *J. Plasma Phys.* **39**, 319 (1988).

8. S.J. Diem, et al., *Rev. Sci. Instrum.* **77** (2006).

9. R.H. Dicke, *Rev. Sci. Instrum.* **17**, 268 (1946).

10. J. Preinhaelter, et al., *Rev. Sci. Instrum.* **77** (2006).

11. A.K. Ram, et al., *Phys. Plasmas* **9**, (2002) 409.

12. J. Urban and J. Preinhaelter, *J. Plasma Phys.* **72** (2006).

13. B.P. LeBlanc, et al., *Rev. Sci. Instrum*. **74** (2003).

14. L. Lao, et al., *Nucl. Fusion* **25**, 1611 (1985).

15. P.L. Bhatnagar, et al., *Physical Review* **94**(3), 511 (1954).

16. E.P. Gross, et al., *Physical Review* **102**(3), 593 (1956).

17. J.B. Wilgen, et al., APS-DPP Conference Proceedings, Long Beach, CA (2001).

18. G.Taylor, et al., *Phys Plasmas* **12**, 052511 (2005).

19. S. Pesic, et al., *Physica* **125C**, 118 (1984).

20. H.W. Kugel, et al., *J. of Nucl. Mat.* **363-365**, 791 (2007).

FIGURE CAPTIONS

Figure 1. B-X-O mode conversion efficiency map, equation (1a), is shown as a function of toroidal and poloidal angle for 15.5 GHz fundamental emission from an L-mode plasma. The center contour represents the angular region where > 90% transmission occurs. Each contour thereafter represents a 10% decrease in the mode conversion efficiency.

Figure 2. Shown is a schematic of the 18-36 GHz dual-channel heterodyne radiometer system.

Figure 3. Shown is a schematic of the 8-18 GHz switched VCO system.

Figure 4. (a) The measured 15.5 GHz fundamental emission during an NSTX discharge. **(b)** The calculated B-X-O mode conversion efficiency (solid line), using the measured L_n (dashed line) in equation (1a), is shown as a function of time.

Figure 5. The time evolution of the **(a)** plasma current, electron temperature and **(b)** EBE (solid line) and B-X-O transmission efficiency (dashed line) for second harmonic emission at 24 GHz. The grey region represents the uncertainty in the EBE measurements.

Figure 6. The measured (solid line) and simulated (dashed lines) EBE for fundamental emission during an NSTX H-mode discharge (124306) is shown as a function of time. Little difference is observed between the simulated T_{rad} without collisional effects (dashed line indicated with X's) and with collisional effects (dotted lines indicated with triangles), suggesting EBW collisional damping is significantly reduced. The shaded grey area represents the uncertainty in the EBE measurements.

Figure 7. The time evolution of the **(a)** plasma current, **(b)** $T_e(0)$ and **(c)** $n_e(0)$ are shown for NSTX H-mode discharge 124303.

Figure 8. The EBE measured $T_e(R)$ ($=T_{rad}/\eta_{B\text{-}X\text{-}O}$) is indicated by the triangles and plotted as a function of major radius for the discharge shown in figure 7 at t = 0.365 s. The radial error bars represent the weighted emission location using 41 rays to simulate the beam waist. The vertical error bars represent the uncertainty in the EBE measurements. The solid line shows the T_e profile from Thomson scattering at t = 0.365 s.

Figure 9. The emission location (solid black) and the harmonic number (dot-dashed) are shown for the 41 rays used in the EBE simulation for 19.5 GHz emission. This frequency had the largest radial extent due to the contributions from fundamental and second harmonic emission locations.

Figure 10. The characteristic frequency plot is shown for H-mode discharge 124303. The first 3 EC harmonics (solid lines) and O-mode cutoff (dashed line) are shown as a

function of major radius. The grey regions surrounding the EC harmonics indicate the Doppler shifted resonance frequency. The light shaded box indicates the frequency range of the radiometer system.

Figure 11. The emission location for the 41 rays used in the EBE simulation code to model the antenna beam waist is shown for 28 GHz (dot-dashed) and 29.5 GHz (black solid) emission.

FIGURES

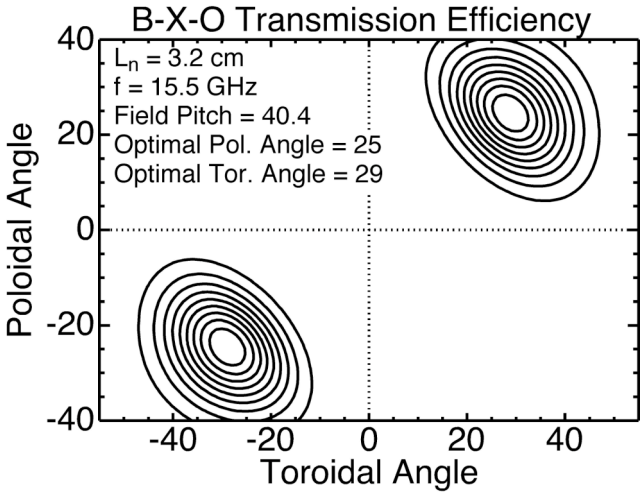

Figure 1.

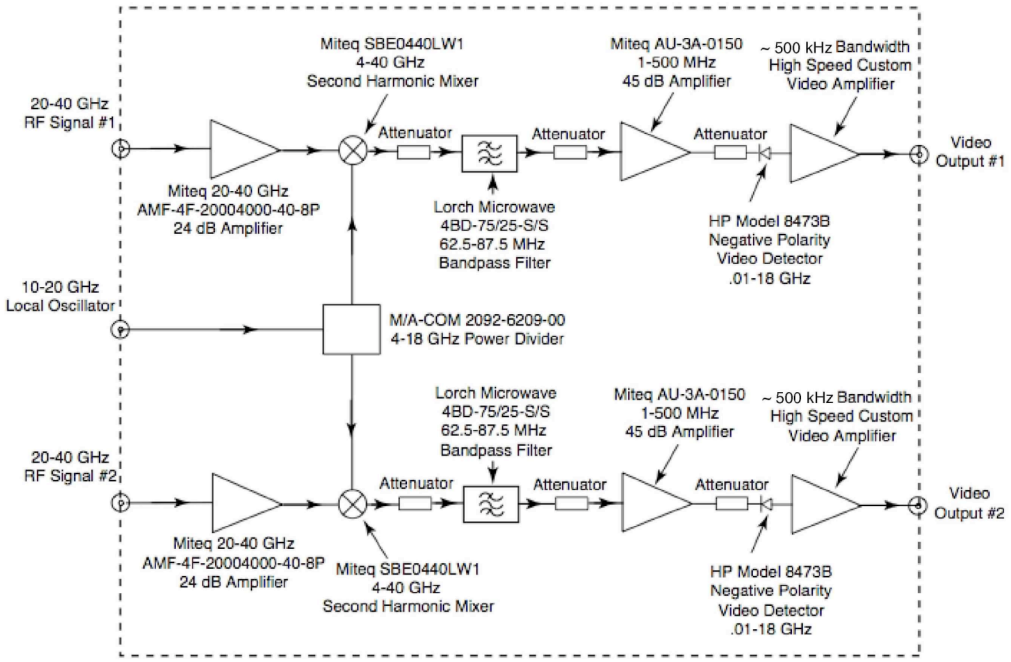

NSTX Dual-Channel 20-40 GHz EBW Radiometer

Figure 2.

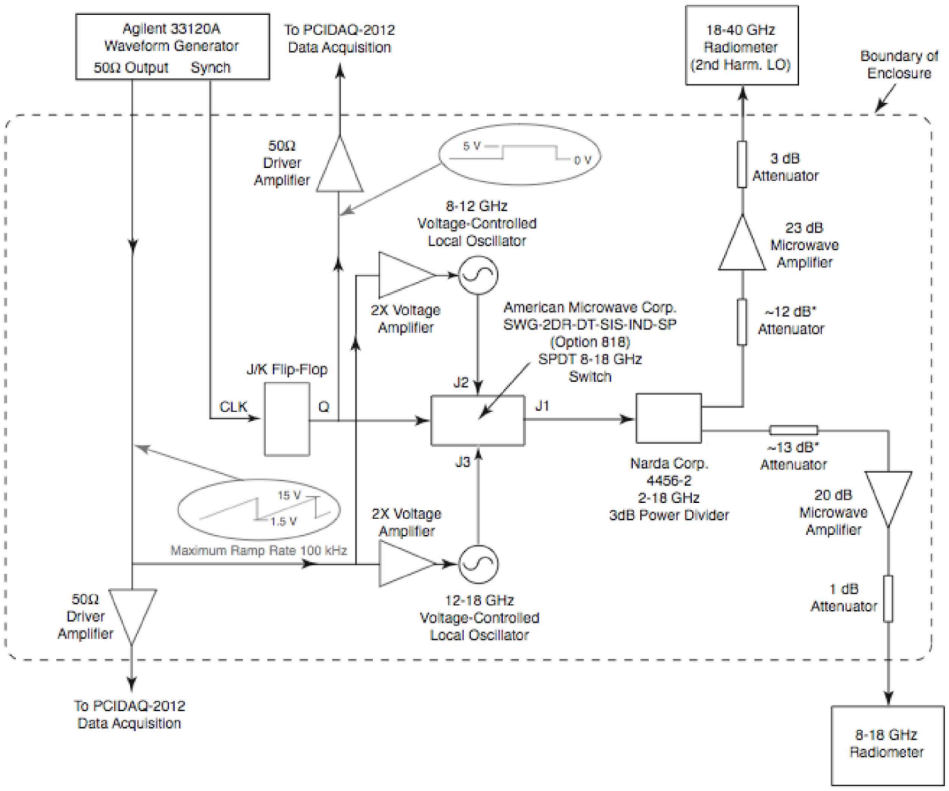

8-18 GHz Switched VCO

Figure 3.

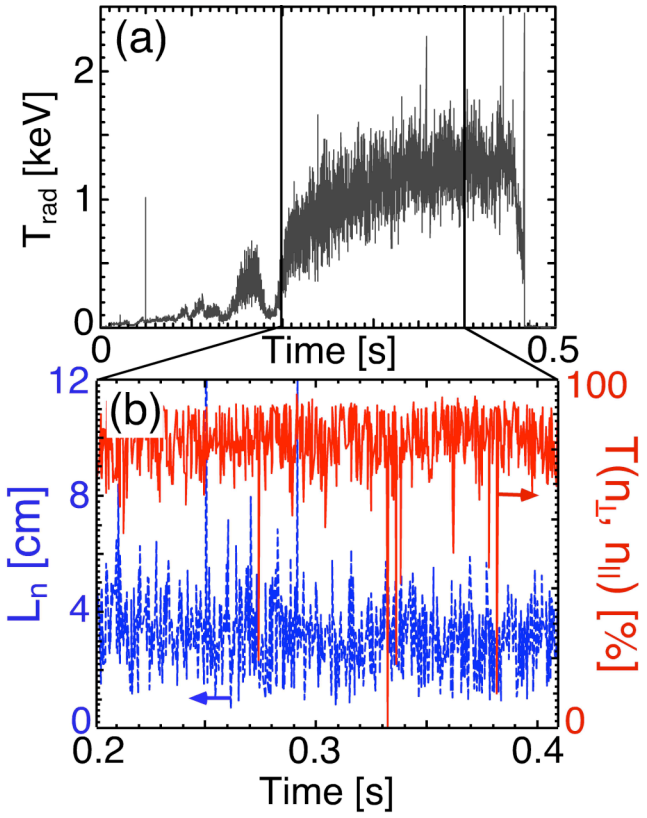
(a)
T_{rad} [keV]
2
1
0
0
Time [s]
0.5
(b)
12
8
4
0
L_n [cm]
100
0
$T(n_\perp, n_\parallel)$ [%]
0.2
0.3
0.4
Time [s]

Figure 4.

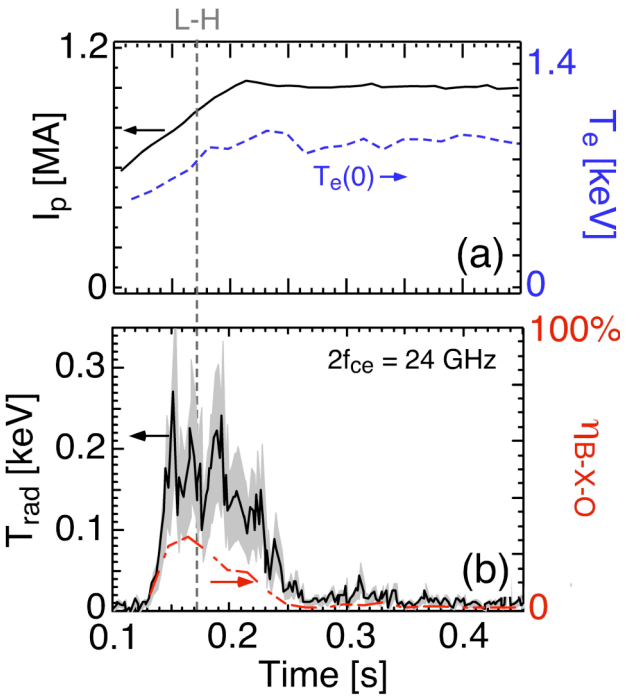
L-H
1.2
0
I_p [MA]
1.4
0
T_e [keV]
$T_e(0)$
(a)
100%
0
$\eta_{B\text{-}X\text{-}O}$
0.3
0.2
0.1
0
T_{rad} [keV]
$2f_{ce}$ = 24 GHz
(b)
0.1
0.2
0.3
0.4
Time [s]

Figure 5.

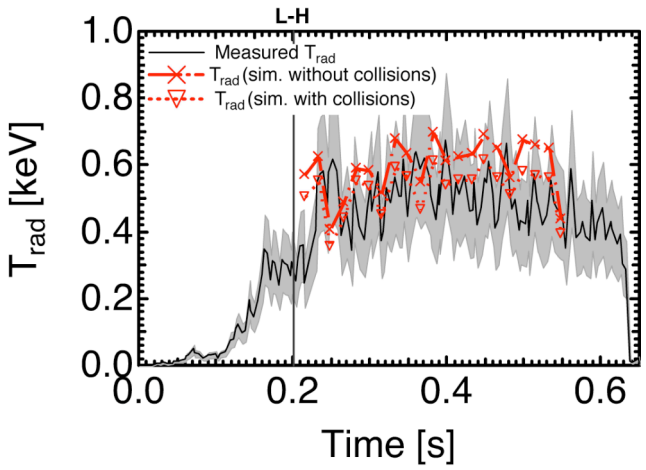
L-H
Measured T_{rad}
T_{rad} (sim. without collisions)
T_{rad} (sim. with collisions)
T_{rad} [keV]
Time [s]
1.0
0.8
0.6
0.4
0.2
0.0
0.0
0.2
0.4
0.6

Figure 6.

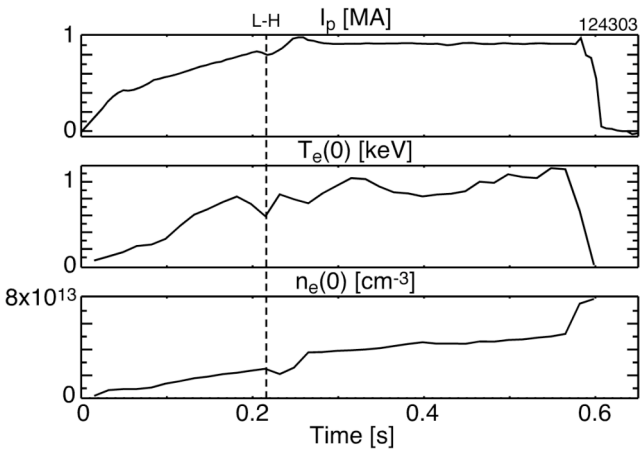

Figure 7.

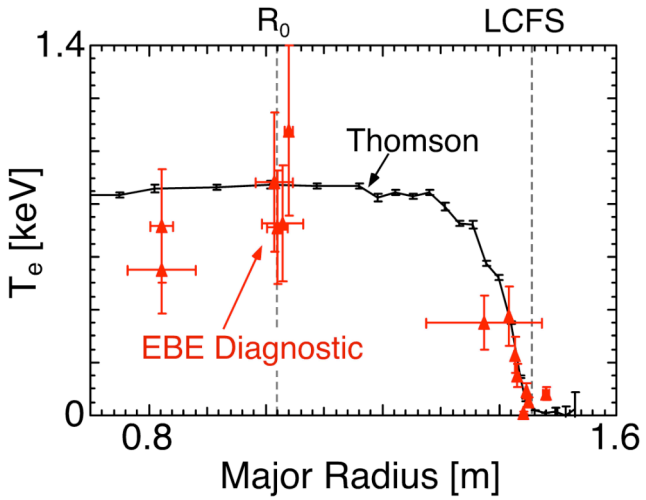
R0
LCFS
1.4
0
Thomson
EBE Diagnostic
Te [keV]
0.8
1.6
Major Radius [m]

Figure 8.

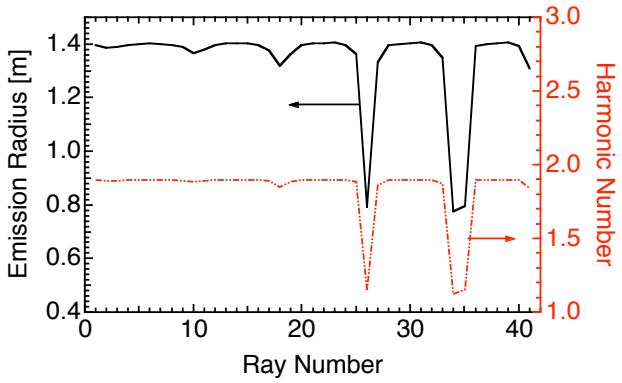
Emission Radius [m]
1.4
1.2
1.0
0.8
0.6
0.4
0
10
20
30
40
Ray Number
3.0
2.5
2.0
1.5
1.0
Harmonic Number

Figure 9.

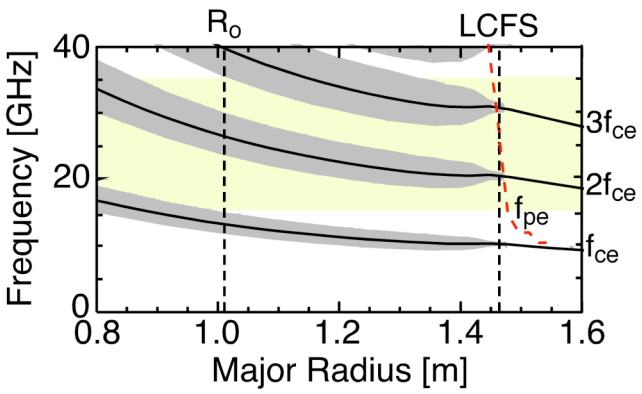
R0
LCFS
40
20
0
Frequency [GHz]
0.8
1.0
1.2
1.4
1.6
Major Radius [m]
3fce
2fce
fpe
fce

Figure 10.

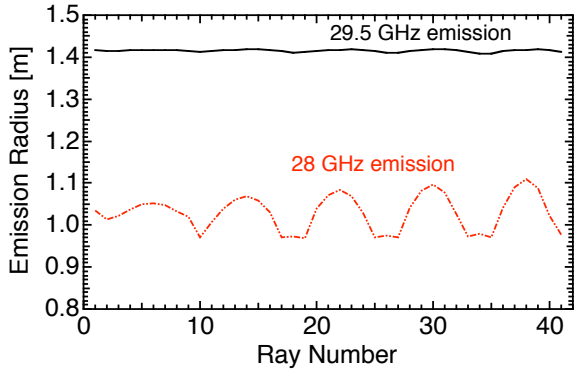
29.5 GHz emission
28 GHz emission
Emission Radius [m]
Ray Number
1.5
1.4
1.3
1.2
1.1
1.0
0.9
0.8
0
10
20
30
40

Figure 11.

The Princeton Plasma Physics Laboratory is operated
by Princeton University under contract
with the U.S. Department of Energy.

Information Services
Princeton Plasma Physics Laboratory
P.O. Box 451
Princeton, NJ 08543

Phone: 609-243-2750
Fax: 609-243-2751
e-mail: pppl_info@pppl.gov
Internet Address: http://www.pppl.gov